Metastability of Diamond Ramp-Compressed to 2 TPa

A. Lazicki,[1] D. McGonegle,[2] J. R. Rygg,[3,4] D. G. Braun,[1] D. C. Swift,[1] M. G. Gorman,[1] R. F. Smith,[1] P. G. Heighway,[2] A. Higginbotham,[5] M. J. Suggit,[2] D. E. Fratanduono,[1] F. Coppari,[1] C. E. Wehrenberg,[1] R. G. Kraus,[1] D. Erskine,[1] J. V. Bernier,[1] J. M. McNaney,[1] R. E. Rudd,[1] G. W. Collins,[3,4] J. H. Eggert,[1] and J. S. Wark[2]

[1]*Lawrence Livermore National Laboratory, 7000 East Ave., Livermore CA 94550 USA*
[2]*Department of Physics, Clarendon Laboratory, University of Oxford, Parks Road, Oxford, OX1 3PU, United Kingdom*
[3]*Laboratory for Laser Energetics, University of Rochester, Rochester, New York 14623-1299, USA*
[4]*Departments of Mechanical Engineering, and Physics and Astronomy, University of Rochester, New York 14623, USA*
[5]*University of York, Department of Physics, Heslington, York YO10 5DD, United Kingdom*

Carbon is the fourth most prevalent element in the universe and essential for all known life. In the elemental form it is found in multiple allotropes including graphite, diamond, and fullerenes, and it has long been predicted that even more structures can exist at greater than Earth-core pressures.[1–3]. Several new phases have been predicted in the multi-terapascal (TPa) regime, important for accurately modeling interiors of carbon-rich exoplanets[4,5]. By compressing solid carbon to 2 TPa (20 million atmospheres; over 5 times the pressure at the Earth's core) using ramp-shaped laser pulses, and simultaneously measuring nanosecond-duration time resolved x-ray diffraction, we found that solid carbon retains the diamond structure far beyond its regime of predicted stability. The results confirm predictions that the strength of the tetrahedral molecular orbital bonds in diamond persists under enormous pressure, resulting in large energy barriers that hinder conversion to the more stable high-pressure allotropes[1,2], just as graphite formation from metastable diamond is kinetically hindered at atmospheric pressure. This work nearly doubles the record high pressure at which x-ray diffraction has been recorded on any material.

On Earth, carbon can exist in a number of different allotropes, with graphite and diamond being the most well-known, although several others exist[6–8], or have been predicted to be stable[9–11]. Diamond, the face-centered-cubic form of carbon (*F43m*, here called FC8) has many technologically important properties owing to its compressive strength and high thermal conductivity. The phase diagram of carbon at pressures in the TPa regime is directly relevant to the structure of planets within our own solar system and beyond[4,5]. Theoretical calculations based on Density Functional Theory (DFT) of the crystalline phases of carbon at TPa-scale pressures have a long history[1–3,12–14], with general agreement emerging that body-centered-cubic (*Ia-3*, called BC8) and simple-cubic (*Pm-3m* called SC1, and $P4_332$, called SC4) phases are lower in enthalpy than FC8 above ∼1 TPa, with BC8 being the first to satisfy this condition around 1 TPa (Figure 1).

Multi-TPa pressures far exceed those that can be achieved under static conditions in the laboratory using anvils[20,21]. While such high pressures can be obtained with shock compression, this highly entropic process starts melting diamond above 0.6 TPa, according to a study of changes in entropy manifested in decaying shock waves[18] (Figure 1). Recently, however, a new dynamic technique known as ramp compression has been developed, in which a sample is compressed on a timescale that is long compared to the sound wave transit time though the sample, thus reducing dissipative processes and keeping the sample cooler than it would be in the shocked state[22]. By use of such a technique diamond has previously been ramp-compressed to record-high pressures (more accurately longitudinal stresses, because of the uniaxial loading) of 5 TPa at the National Ignition Facility (NIF)[23]. This ramp data gave no in-

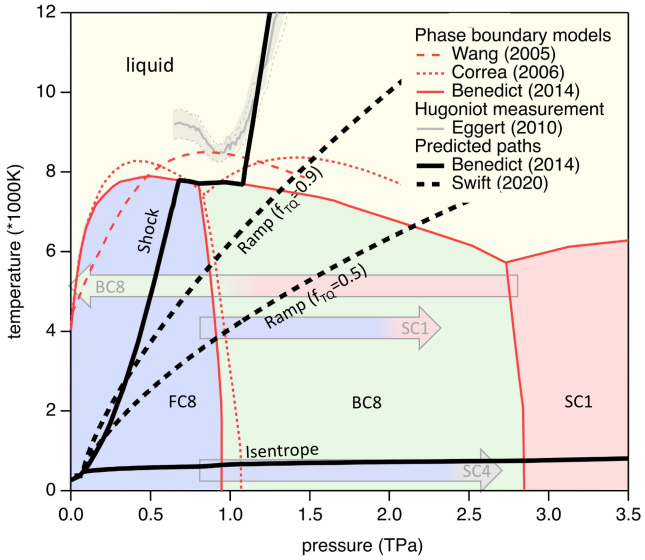

FIG. 1. **Carbon phase diagram summarizing DFT-predicted phase boundaries[15–17], Hugoniot data[18], and predicted thermodynamic paths[17,19]** | The broad arrows represent the predicted structural evolution if kinetic effects are taken into account[2]. The two proposed ramp paths show the effect of different fractions of plastic work appearing as heat, described by the Taylor-Quinney factor (f_{TQ})[19]. The observation in this study of solid FC8 carbon at 2 TPa suggests that strength may be lower than predicted or that plastic work is contributing largely to microstructural changes rather than heating.

dicators of a phase transformation, such as plateaus in the velocity ramp due to changes in sound speed. A second experimental study has interpreted subtle trends in shock Hugoniot data near the melting point as evidence for the FC8-BC8-liquid triple point near 1 TPa[24]. However, neither of these studies included a measurement of structure.

In fact, whether and how diamond might actually transform to one of the predicted phases in a laboratory compression experiment are far from trivial questions to answer, owing to the large enthalpy barriers predicted between the phases (a phenomenon that explains the very existence of ambient-pressure diamond itself, given its metastability compared with graphite). Simulations at zero Kelvin report that the predicted BC8 phase will never form under rapid compression, and the FC8 phase will persist until it becomes mechanically unstable near 3 TPa[1]. At high temperature however the atoms are freed to follow alternative transformation pathways and the enthalpy of formation is lower for some phases. At 2 TPa and 4000 K FC8 is predicted to transform to the lower energy (but still metastable) SC1 phase, and at 300 K and 2.5 TPa to another metastable SC4 structure[2]. It is also predicted that BC8 will form at ~1 TPa, but only under release from the SC1 phase. To explore this rich and complex landscape, it is necessary to couple the most powerful pressure drivers with *in-situ* probes of structure.

In conjunction with dynamic ramp compression using laser ablation, quasi-monochromatic x-ray emission can be produced by irradiating separate targets at high laser intensities[25,26], and these x-rays used for x-ray diffraction[27] and structural determination[28] during the nanosecond compression. We have now implemented this technique at the NIF[29], making it possible for the first time to tackle multi-TPa measurements of structure. Here we report the results of diamond ramp-compression experiments to 2 TPa with simultaneous x-ray diffraction measurements of structure. This stress state is the highest at which x-ray diffraction information has ever been obtained, and we find that diamond remains solid and retains the FC8 phase.

As described in the methods section, we used laser ablation to ramp compress samples of pure polycrystalline diamond or diamond-epoxy aggregates (for shots N150217 and N150927), to stress states between 0.8 and 2 TPa for a duration of several nanoseconds. During the time of peak compression, separate laser beams were focused onto either Ge or Zr foils offset from the diamond target, to create a bright quasi-monochromatic x-ray source with energies of 10.25 keV (Ge) or 16.25 keV(Zr). The x rays scattered from the compressed diamond were collimated by a pinhole placed just behind the sample itself. The sample sat on the surface of a hollow container lined with image plates, such that the diffracted signal in transmission was recorded over almost a full 2π steradians, providing Debye-Scherrer diffraction patterns (Extended Data Figure 1). On each shot the velocity history of the rear surface of the target is

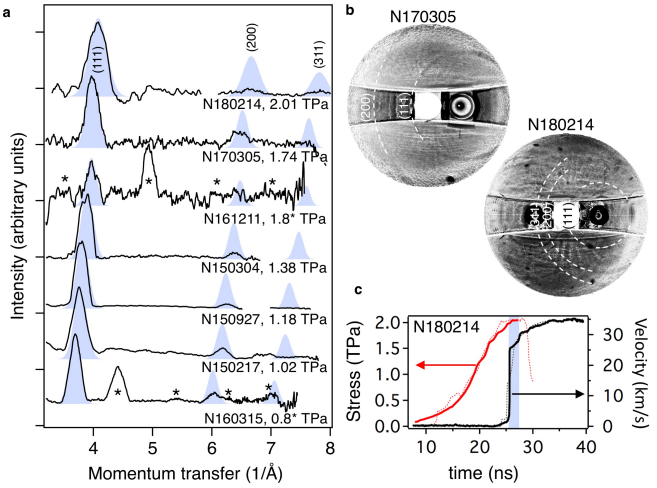

FIG. 2. **Summary of experimental data** | **a**, X-ray diffraction lineouts (black) and ideal FC8 diffraction patterns (blue, described in the Extended Data Figure 2). The data processing in the presence of high noise at the highest pressures is illustrated in Extended Data Figures 6 and 7. Asterisks mark the position of B2 MgO diffraction peaks. Stereographic projections of the background-subtracted image plates for shots N170305 (10.25 keV x-rays) and N180214 (16.25 keV x-rays) are shown in **b**, with carbon peaks marked with white arc segments. The velocity history and inferred pressure for shot N180214 **c** (solid lines) agree well with radiation-hydrodynamic predictions (dashed)[32]. The compression wave is a smooth ramp within the sample and steepens to a shock by the time it reaches the measured surface. The blue band illustrates the timing of the x-ray source.

recorded via VISAR (Velocity Interferometer System for Any Reflector)[30]. A characteristics analysis is used to translate these velocity data into a stress-density history within the target[31]. The Debye-Scherrer pattern at 1.74 and 2 TPa is shown in Figure 2 (and the rest summarized in the Extended Data Figures 2 and 3) along with azimuthally-averaged lineouts for all reported shots. The background subtraction algorithms and means of accurately determining the scattering angle are described in detail elsewhere[29] and illustrated in Extended Data Figure 6. The diffraction peaks in the lineouts are fit with a gaussian function and the best-fit peak centroids used in a least-squares fitting to determine the density.

At 0.8 TPa the (111), (200) and (311) diffraction peaks from the FC8 structure are identifiable. As the stress increases the scattering angle for the (311) peak approaches the edge of the image plate, and between 1-2 TPa, only the (111) and (220) peaks are reliably seen. Peak positions and deduced densities shown in Figure 3, (summarized in Extended Data Table 1) are in good agreement with previous measurements[23,33]. In Figure 3 we also show the angular positions at which we would expect diffraction from the BC8, SC1 and SC4 structures. None of the data shows evidence of these new phases. Some additional peaks (marked with asterisks) are identified

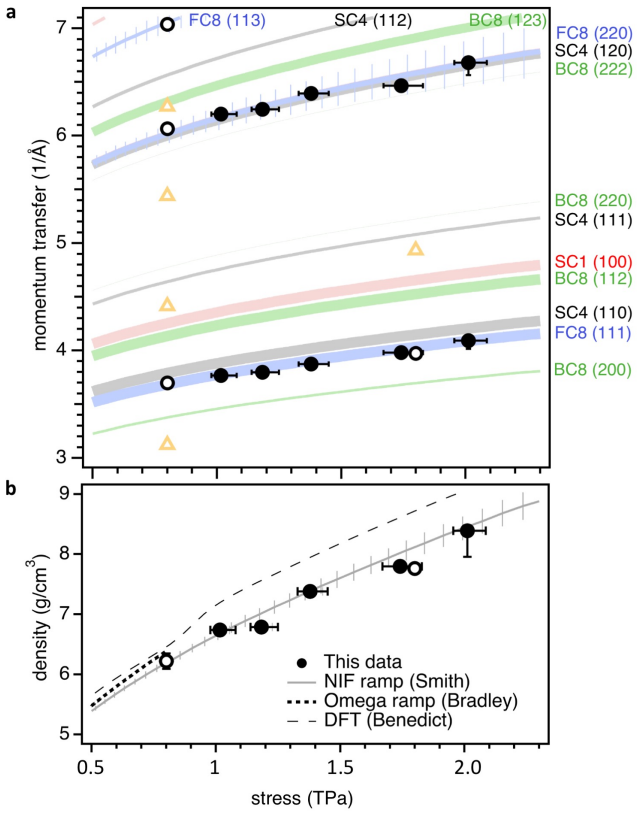

FIG. 3. **Data compared to theoretical predictions** | **a**, Position of carbon diffraction peaks (black circles, error bars defined in the Methods section) compared with predictions for candidate phases (solid curves with widths proportional to ideal intensities normalized to the most intense peak). Diffraction from the B2 phase of MgO (yellow triangles) was observed in the two experiments. Reported stress was deduced from VISAR measurements (solid markers), or radiation-hydrodynamic simulations (open markers)[32]. The compressibility of the predicted carbon phases is taken from the NIF experimental results[23] and the associated uncertainty shown as error bars on the predicted FC8 lines. **b** Inferred density from best fit FC8 structure, compared with the published ramp equations of state[23,33] and a DFT-based model[17].

with MgO[34] in a subset of the shots where single-crystal MgO was used as a window material (more information in the Supplemental Materials).

The most likely reason we did not observe the BC8 phase is the high enthalpy barrier caused by the large number of strong sp^3 bonds that must be broken to change the structure. The FC8 and BC8 phases are shown in Figure 4 and, while both can be viewed as layers of sp^3-bonded carbon in 6-member rings, there is no simple shift that will transform one to another. The FC8 layers are bound by zigzag interlayer bonds, which give the structure its distinctive open channels. The BC8 interlayer bonds form helical chains and adjacent layers are consequently shifted, eliminating the open channels. Mechanisms for the transformation have been suggested which require a minimum of 1.5 bonds/atom

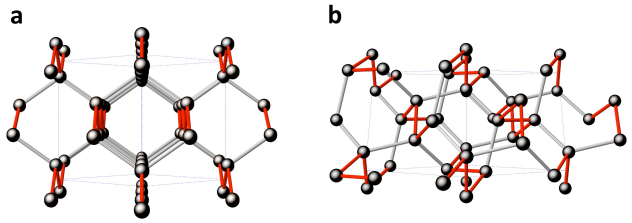

FIG. 4. **FC8 and BC8 crystal structures** | Both are represented in the rhombohedral space group $\bar{R}3$ (C_2^3, no. 148) with occupied 2c and 6f Wykoff sites, which was identified as the correspondence requiring the minimum number of broken sp^3 bonds (1.5 per atom)[9]. Highlighted in red are sp^3 bonds that connect the layers. **a** The FC8 structure with simple zig-zag interlayer bonding (red) defining the 110 channels. **b** The BC8 structure with significantly more complex helical interlayer bonding (red) and lack of distinct channels.

to be broken[9]; a considerable energy cost due to the stability of the sp^3 bond. This observation is analogous to the case of carbon's sp^3-bonded group-14 neighbors Si and Ge which, absent a chemical reaction or application of significant heat, only transform to the BC8 structure upon release from a higher pressure phase[35,36]. Carbon's sp^3 bonds are even stronger however, due to the lack of p electrons in the atomic core[12]. The predicted enthalpy barrier of ~2.5 eV/atom between FC8 and BC8[2,9] is approaching the barrier between metastable FC8 and stable graphite phases at ambient conditions, and that transformation, while spontaneous, takes geologic timescales. Consequently, it may not be surprising that we do not observe the FC8-BC8 transition in our ~10-ns ramp-compression experiments. The predicted enthalpy barrier between hexagonal diamond (observed to form from shocked graphite[37]) and BC8 is lower at ~1 eV[9], suggesting another route to explore for formation of BC8.

Not yet considered in this discussion is the role of temperature, which can open up new transformation pathways and overcome kinetic barriers. The prediction that the kinetic barrier between FC8 and metastable SC1 could be surmounted at 2TPa and 4000 K[2] was potentially within our reach to test, depending on the temperature in the experiment. A lower bound on the temperature can be estimated from the heating associated with a shock to ~1 Mbar (the elastic limit of diamond[38]) which was observed on all shots, followed by an isentrope, as illustrated in Figure 1. In the dynamic technique, however, hydrostatic conditions are approached within the sample as the shear stress is relieved by plastic flow, with an associated conversion of the plastic work to heat[22,33]. The strength of the material, which determines residual shear stress, thus plays a key role in the final temperature. Strength models for diamond based on DFT calculations of the elastic moduli as a function of compression[19,39] indicate that a ramp-compressed diamond sample will be well above the predicted melting temperature by 2 TPa, if we assume that most of the

plastic work is converted to heat. The fact that solid x-ray diffraction is observed in this experiment at 2 TPa suggests that either the strength is lower than expected (some experimental evidence has already been put forward which indicates that diamond has a maximum resolved shear stress which is much lower than theoretical predictions[38,40]), or that a large percentage of plastic work must be accounted for some other way. This fraction of plastic work which shows up as heat, traditionally represented by the Taylor-Quinney factor (f_{TQ})[41], is usually assumed to be near 0.9 for metals, and the remainder goes toward microstructural changes like creating defects, which can be very numerous at high strain rates[42]. Within this simplified model, f_{TQ} should be nearer to 0.5 for carbon to remain solid at 2 TPa (Figure 1)[19], if the predicted melting curve is accurate at these conditions. In reality, the evolution of lattice defects and strength in carbon along a ramp-compression pathway is likely to be complex and certain to be time-varying, and a detailed energy-budget analysis, as has been done for the case of Ta[43], would be fruitful.

A reliable temperature determination, which is currently lacking, would allow this data to be used directly to benchmark improved models for diamond strength, phase diagram and phase transformation kinetics under ramp conditions. These results highlight the crucial importance of developing techniques compatible with dynamic experiments for measuring temperature. While some progress has been made by employing the Debye-Waller effect in EXAFS[44] and diffraction measurements[45], high-quality, untextured diffraction data is required, and the uncertainties in the derived values are extremely high. With the advent of high-power, high-rep-rate lasers[46] coupled to ultra-high brightness free-electron-laser x-ray sources[47,48], it may become possible to drive diamond to the TPa pressure range and probe structure as well as temperature, using alternative techniques such as inelastic x-ray scattering[49].

Using x-ray diffraction we have for the first time directly probed the crystal structure of diamond in the pressure regime where several phases are predicted to be more stable than the well-known FC8 structure. Our data show no evidence for a phase transformation between 0.8 and 2 TPa, the highest-pressure diffraction measurement ever reported. The persistence of the metastable FC8 phase up to 1 TPa beyond its predicted phase boundary gives further evidence for the extraordinary strength and stability of the carbon sp^3 bond. The observation of solid ramp-compressed diamond at 2 TPa also sets a bound for models of the melt curve, strength and degree of plastic work converted to heat.

ACKNOWLEDGEMENTS

We gratefully acknowledge helpful discussions with Bruce Remington, Marius Millot and Dennis Klug, and we thank the NIF staff and the NIF Discovery Science program. This work was performed under the auspices of the U.S. Department of Energy by Lawrence Livermore National Laboratory under Contract No. DE-AC52-07NA27344. JSW is grateful to the UK EPSRC for support under grants EP/J017256/1 and EP/S025065/1. D.M. was supported by LLNS under contract number B595954.

[1] S. Scandolo, G. L. Chiarotti, and E. Tosatti, "SC4: A metallic phase of carbon at terapascal pressures," Phys. Rev. B **53**, 5051–5054 (1996).

[2] Jian Sun, Dennis D. Klug, and Roman Martoňák, "Structural transformations in carbon under extreme pressure: Beyond diamond," The Journal of Chemical Physics **130**, 194512 (2009).

[3] Miguel Martinez-Canales, Chris J. Pickard, and Richard J. Needs, "Thermodynamically stable phases of carbon at multiterapascal pressures," Phys. Rev. Lett. **108**, 045704 (2012).

[4] Nikku Madhusudhan, Kanani K. M. Lee, and Olivier Mousis, "A possible carbon-rich interior in super-earth 55 Cancri e," Astrophys. J. **759**, L40 (2012), arXiv:1210.2720 [astro-ph.EP].

[5] Natalie Mashian and Abraham Loeb, "CEMP stars: possible hosts to carbon planets in the early universe," Monthly Notices of the Royal Astronomical Society **460**, 2482–2491 (2016).

[6] Clifford Frondel and Ursula B. Marvin, "Lonsdaleite, a hexagonal polymorph of diamond," Nature **214**, 587–589 (1967).

[7] Jagdish Narayan and Anagh Bhaumik, "Novel phase of carbon, ferromagnetism, and conversion into diamond," Journal of Applied Physics **118**, 215303 (2015).

[8] Roy L. Johnston and Roald Hoffmann, "Superdense carbon, C8: supercubane or analog of γ-silicon?" Journal of the American Chemical Society **111**, 810–819 (1989).

[9] C. Mailhiot and A. K. McMahan, "Atmospheric-pressure stability of energetic phases of carbon," Phys. Rev. B **44**, 11578–11591 (1991).

[10] Artem R. Oganov and Colin W. Glass, "Crystal structure prediction using ab initio evolutionary techniques: Principles and applications," The Journal of Chemical Physics **124**, 244704 (2006).

[11] Artem R. Oganov, Russell J. Hemley, Robert M. Hazen, and Adrian P. Jones, "Structure, bonding, and mineralogy of carbon at extreme conditions," Reviews in Mineralogy and Geochemistry **75**, 47–77 (2013).

[12] M. T. Yin and Marvin L. Cohen, "Will diamond transform under megabar pressures?" Phys. Rev. Lett. **50**, 2006–2009 (1983).

[13] R. Biswas, Richard M. Martin, R. J. Needs, and O. H. Nielsen, "Stability and electronic properties of complex structures of silicon and carbon under pressure: Density-

functional calculations," Phys. Rev. B **35**, 9559–9568 (1987).
[14] S. Fahy and Steven G. Louie, "High-pressure structural and electronic properties of carbon," Phys. Rev. B **36**, 3373–3385 (1987).
[15] Xiaofei Wang, Sandro Scandolo, and Roberto Car, "Carbon phase diagram from ab initio molecular dynamics," Phys. Rev. Lett. **95**, 185701 (2005).
[16] Alfredo A. Correa, Stanimir A. Bonev, and Giulia Galli, "Carbon under extreme conditions: Phase boundaries and electronic properties from first-principles theory," Proceedings of the National Academy of Sciences **103**, 1204–1208 (2006).
[17] Lorin X. Benedict, Kevin P. Driver, Sebastien Hamel, Burkhard Militzer, Tingting Qi, Alfredo A. Correa, A. Saul, and Eric Schwegler, "Multiphase equation of state for carbon addressing high pressures and temperatures," Phys. Rev. B **89**, 224109 (2014).
[18] J. H. Eggert, D. G. Hicks, P. M. Celliers, D. K. Bradley, R. S. McWilliams, R. Jeanloz, J. E. Miller, T. R. Boehly, and G. W. Collins, "Melting temperature of diamond at ultrahigh pressure," Nature Physics **6**, 40–43 (2009).
[19] D. C. Swift, O Heuzé, A Lazicki, S. Hamel, L. X. Benedict, R. F. Smith, J. M. McNaney, and G. J. Ackland, "Equation of state and strength of diamond in high pressure ramp loading," arXiv:2004.03071 (2020).
[20] Leonid Dubrovinsky, Natalia Dubrovinskaia, Vitali B. Prakapenka, and Artem M. Abakumov, "Implementation of micro-ball nanodiamond anvils for high-pressure studies above 6 Mbar," Nature Communications **3**, 1163 (2012), article.
[21] Hao Wu, Xudong Luo, Libin Wen, Hong Sun, and Changfeng Chen, "Extreme static compression of carbon to terapascal pressures," Carbon **144**, 161–170 (2019).
[22] Damian C. Swift, "Numerical solution of shock and ramp compression for general material properties," Journal of Applied Physics **104**, 073536 (2008).
[23] R. F. Smith, J. H. Eggert, R. Jeanloz, T. S. Duffy, D. G. Braun, J. R. Patterson, R. E. Rudd, J. Biener, A. E. Lazicki, A. V. Hamza, J. Wang, T. Braun, L. X. Benedict, P. M. Celliers, and G. W. Collins, "Ramp compression of diamond to five terapascals," Nature **511**, 330–333 (2014).
[24] M. D. Knudson, M. P. Desjarlais, and D. H. Dolan, "Shock-wave exploration of the high-pressure phases of carbon," Science **322**, 1822–1825 (2008).
[25] M. A. Barrios, S. P. Regan, K. B. Fournier, R. Epstein, R. Smith, A. Lazicki, R. Rygg, D. E. Fratanduono, J. Eggert, H.-S. Park, C. Huntington, D. K. Bradley, O. L. Landen, and G. W. Collins, "X-ray area backlighter development at the National Ignition Facility (invited)," Review of Scientific Instruments **85**, 11D502 (2014).
[26] F. Coppari, R. F. Smith, D. B. Thorn, J. R. Rygg, D. A. Liedahl, R. G. Kraus, A. Lazicki, M. Millot, and J. H. Eggert, "Optimized x-ray sources for x-ray diffraction measurements at the Omega Laser Facility," Review of Scientific Instruments **90**, 125113 (2019).
[27] Justin S. Wark, Robert R. Whitlock, Allan A. Hauer, James E. Swain, and Paul J. Solone, "Subnanosecond x-ray diffraction from laser-shocked crystals," Phys. Rev. B **40**, 5705–5714 (1989).
[28] J. R. Rygg, J. H. Eggert, A. E. Lazicki, F. Coppari, J. A. Hawreliak, D. G. Hicks, R. F. Smith, C. M. Sorce, T. M. Uphaus, B. Yaakobi, and G. W. Collins, "Powder diffraction from solids in the terapascal regime," Review of Scientific Instruments **83**, 113904 (2012), https://doi.org/10.1063/1.4766464.
[29] J. R. Rygg, R. F. Smith, A. E. Lazicki, D. G. Braun, D. E. Fratanduono, R. G. Kraus, J. M. McNaney, D. C. Swift, C. E. Wehrenberg, F. Coppari, M. F. Ahmed, M. A. Barrios, K. J. M. Blobaum, G. W. Collins, A. L. Cook, P. Di Nicola, E. G. Dzenitis, S. Gonzales, B. F. Heidl, M. Hohenberger, A. House, N. Izumi, D. H. Kalantar, S. F. Khan, T. R. Kohut, C. Kumar, N. D. Masters, D. N. Polsin, S. P. Regan, C. A. Smith, R. M. Vignes, M. A. Wall, J. Ward, J. S. Wark, T. L. Zobrist, A. Arsenlis, and J. H. Eggert, "X-ray diffraction at the National Ignition Facility," Review of Scientific Instruments **91**, 043902 (2020).
[30] P. M. Celliers, D. K. Bradley, G. W. Collins, D. G. Hicks, T. R. Boehly, and W. J. Armstrong, "Line-imaging velocimeter for shock diagnostics at the OMEGA laser facility," Review of Scientific Instruments **75**, 4916–4929 (2004), https://doi.org/10.1063/1.1807008.
[31] S D Rothman, J-P Davis, J Maw, C M Robinson, K Parker, and J Palmer, "Measurement of the principal isentropes of lead and lead–antimony alloy to ∼400 kbar by quasi-isentropic compression," Journal of Physics D: Applied Physics **38**, 733–740 (2005).
[32] G. Zimmerman, D. Kershaw, D. Bailey, and J. Harte, "LASNEX code for inertial confinement fusion," J. Opt. Soc. Am. **68**, 549 (1978).
[33] D. K. Bradley, J. H. Eggert, R. F. Smith, S. T. Prisbrey, D. G. Hicks, D. G. Braun, J. Biener, A. V. Hamza, R. E. Rudd, and G. W. Collins, "Diamond at 800 GPa," Phys. Rev. Lett. **102**, 075503 (2009).
[34] F. Coppari, R. F. Smith, J. H. Eggert, J. Wang, J. R. Rygg, A. Lazicki, J. A. Hawreliak, G. W. Collins, and T. S. Duffy, "Experimental evidence for a phase transition in magnesium oxide at exoplanet pressures," Nature Geoscience **6**, 926–929 (2013).
[35] R. J. Nelmes, M. I. McMahon, N. G. Wright, D. R. Allan, and J. S. Loveday, "Stability and crystal structure of BC8 germanium," Phys. Rev. B **48**, 9883–9886 (1993).
[36] Oleksandr O. Kurakevych, Yann Le Godec, Wilson A. Crichton, Jérémy Guignard, Timothy A. Strobel, Haidong Zhang, Hanyu Liu, Cristina Coelho Diogo, Alain Polian, Nicolas Menguy, Stephen J. Juhl, and Christel Gervais, "Synthesis of bulk BC8 silicon allotrope by direct transformation and reduced-pressure chemical pathways," Inorganic Chemistry **55**, 8943–8950 (2016), pMID: 27532223.
[37] Stefan J. Turneaure, Surinder M. Sharma, Travis J. Volz, J. M. Winey, and Yogendra M. Gupta, "Transformation of shock-compressed graphite to hexagonal diamond in nanoseconds," Science Advances **3**, eaao3561 (2017).
[38] R. S. McWilliams, J. H. Eggert, D. G. Hicks, D. K. Bradley, P. M. Celliers, D. K. Spaulding, T. R. Boehly, G. W. Collins, and R. Jeanloz, "Strength effects in diamond under shock compression from 0.1 to 1 TPa," Phys. Rev. B **81**, 014111 (2010).
[39] Daniel Orlikowski, Alfredo A. Correa, Eric Schwegler, and John E. Klepeis, "A Steinberg-Guinan model for high-pressure carbon: diamond phase," AIP Conference Proceedings **955**, 247–250 (2007).
[40] J. M. Lang, J. M. Winey, and Y. M. Gupta, "Strength and deformation of shocked diamond single crystals: Orientation dependence," Phys. Rev. B **97**, 104106 (2018).
[41] Geoffrey Ingram Taylor and H. Quinney, "The latent energy remaining in a metal after cold working," Proceed-

ings of the Royal Society of London. Series A, Containing Papers of a Mathematical and Physical Character **143**, 307–326 (1934).
[42] M. J. Suggit, A. Higginbothm, J. A. Hawreliak, G. Mogni, G. Kimminau, P. Dunne, A. J. Comley, N. Park, B. A. Remington, and J. S. Wark, "Nanosecond white-light Laue diffraction measurements of dislocation microstructure in shock-compressed single-crystal copper," Nature Communications **3**, 1224 (2012).
[43] P. G. Heighway, M. Sliwa, D. McGonegle, C. Wehrenberg, C. A. Bolme, J. Eggert, A. Higginbotham, A. Lazicki, H. J. Lee, B. Nagler, H.-S. Park, R. E. Rudd, R. F. Smith, M. J. Suggit, D. Swift, F. Tavella, B. A. Remington, and J. S. Wark, "Nonisentropic release of a shocked solid," Phys. Rev. Lett. **123**, 245501 (2019).
[44] Y. Ping, F. Coppari, D. G. Hicks, B. Yaakobi, D. E. Fratanduono, S. Hamel, J. H. Eggert, J. R. Rygg, R. F. Smith, D. C. Swift, D. G. Braun, T. R. Boehly, and G. W. Collins, "Solid iron compressed up to 560 GPa," Phys. Rev. Lett. **111**, 065501 (2013).
[45] William J. Murphy, Andrew Higginbotham, Justin S. Wark, and Nigel Park, "Molecular dynamics simulations of the Debye-Waller effect in shocked copper," Phys. Rev. B **78**, 014109 (2008).
[46] Klaus Ertel, Saumyabrata Banerjee, Paul Mason, P. Phillips, R. Greenhalgh, Cristina Hernandez-Gomez, and John Collier, "DiPOLE: A scalable laser architecture for pumping multi-Hz PW systems," Proc SPIE **8780**, 288–292 (2013).
[47] Gerd Priebe, Motoaki Nakatsutsumi, Ian Thorpe, Benjamin Mueller, Alexander Pelka, Karen Appel, Thomas Tschentscher, and Maximilian Lederer, "High energy/intensity lasers for HED science at European XFEL," Proceedings of NWP-2014, 119 (2014).
[48] C Pellegrini, "X-ray free-electron lasers: from dreams to reality," Physica Scripta **T169**, 014004 (2016).
[49] E. E. McBride, T. G. White, A. Descamps, L. B. Fletcher, K. Appel, F. P. Condamine, C. B. Curry, F. Dallari, S. Funk, E. Galtier, M. Gauthier, S. Goede, J. B. Kim, H. J. Lee, B. K. Ofori-Okai, M. Oliver, A. Rigby, C. Schoenwaelder, P. Sun, Th. Tschentscher, B. B. L. Witte, U. Zastrau, G. Gregori, B. Nagler, J. Hastings, S. H. Glenzer, and G. Monaco, "Setup for meV-resolution inelastic x-ray scattering measurements and x-ray diffraction at the matter in extreme conditions endstation at the Linac Coherent Light Source," Review of Scientific Instruments **89**, 10F104 (2018).
[50] J C Boettger, "Sesame equation of state for epoxy," 10.2172/10131920.
[51] Ch. Wild, N. Herres, and P. Koidl, "Texture formation in polycrystalline diamond films," Journal of Applied Physics **68**, 973–978 (1990), https://doi.org/10.1063/1.346663.
[52] C. Krauland, Private Communication (2019)

METHODS

Target Details: Materials, part thicknesses and assembly are shown in Extended Data Table 1 and Figure 1. We used two types of diamond samples for this study: $\sim$50μm-thick layers of monocrystalline diamond powder embedded in epoxy, and 30-100 μm-thick plates of microcrystalline diamond. The diamond-epoxy composite targets had a packing fraction of 0.53 diamond, approaching the maximally random jammed packing fraction of 0.64. The diamond was a monocrystalline powder with grain size between 50-100 nm, and the epoxy was Stycast 1266, vacuum-outgassed prior to mixing.

There is a significant impedance-mismatch between diamond and epoxy, meaning the compression wave will drop to a much lower pressure when it passes from diamond to epoxy, sending a release wave back into the diamond. However, with grain-sizes of 50-100 nm and sound speeds of at least 3 km/s, the pressure in a grain will equilibrate with the neighboring diamond grains in about 30 ps or faster; much faster than the duration of the 25 ns ramp pulse, and the sample pressure and density will evolve along very close to the same path as the full-density diamond. The motivation for using a slurry rather than full-density diamond sample was based on the expectation, from available strength models and from some experimental efforts on the Omega laser facility, that plastic work heating would cause the diamond ramp to cross the melting line by 8-12 Mbar. The epoxy was intended to reduce the deviatoric stress imposed on the diamond, and also to allow heat to rapidly conduct away from the diamond. The actual effect of the presence of epoxy on the sample temperature depends on the thermal conductivity, which is not well known under these conditions. In the limit of zero conductivity, the diamond temperature will be at most that of full-density diamond. In the limit of infinite conductivity, the temperature rise may follow a path similar to an isentrope in the epoxy, which can be estimated using an equation of state model. The SESAME 7603 model equation of state[50] suggest that temperature may reach 2500 K by 1.2 TPa, lower than the predicted temperature of the full-density diamond (Figure 1). As it became necessary to maximize the diamond volume in order to increase the diffraction signal above the increasing drive background at the highest stresses, we experimented with full-density microcrystalline diamond samples. We found that the samples did not in fact melt as expected, and the slurry target style was subsequently abandoned.

The microcrystalline diamond samples were prepared by Diamond Materials GmbH using chemical vapor deposition (CVD). The ambient material has large (>1 um) grain sizes and a 110 fiber texture[51].

The sample was sandwiched between an ablator package towards the laser drive and a tamper towards the diagnostic. The ablator is composed of a beryllium plate which the lasers irradiate to generate the pressure drive. The laser ablation also generates a broad spectrum of low-energy x-rays peaked around 2 keV. Unshielded, these x-rays heat the diamond sample prior to compression, and also contribute to a high image plate background. A layer of absorbing material (Au or Zr) is therefore sandwiched between the ablator and the diamond sample to absorb these x-rays. A single-crystal diamond or MgO plate positioned on the other side of

the sample functions to delay the arrival of waves that originate at the vacuum interface and drop the pressure to zero.

Laser Configuration The experiments were performed at the National Ignition Facility. Samples were compressed up to 2 TPa using 16 laser beams with their pulses shaped to ramp the total laser intensity from 0 to as high as 500 TW cm^{-2} over 25-30 ns (Extended Data Figure 4). The beam profiles were smoothed using continuous phase plates with *sim*1 mm circular profiles, which were further smoothed using spectral dispersion and orthogonal polarization. The peak laser intensity was maintained for about 5 ns, while a 2-ns-long burst of quasi-monochromatic x-rays illuminated the compressed sample and was diffracted onto image plates. The x-rays were generated by irradiating a foil of Ge or Zr, placed ∼32 mm from the sample, with up to 24 laser beams at an intensity of ∼ 7.5 x 10^{15} W cm^{-2}. The lasers ionize the metal and helium-like emission lines are generated into 4π from the plasma, with energies of 10.25 keV (Ge) or 16.19 keV (Zr), with 1% bandwidth owing to two main transitions being present (1s2p ^{1}P - 1s^2 ^{1}S, and 1s2p ^{3}P - 1s^2 ^{1}S)[25]. The x-ray fluence at the sample is ∼30 x 10^{18} photons/m^2. X-rays that scatter off the sample are collimated by a 400 μm pinhole made of uranium-6wt% niobium alloy placed behind the sample.

Stress state determination The stress state reached in the samples is determined by measuring the velocity of the free surface of the diamond tamper using a velocimetry diagnostic VISAR (Velocity Interferometer System for Any Reflector)[30]. For shots below 1.5 TPa, etalons with sensitivity of 3.1251 km/s/fringe and 5.4603 km/s/fringe were used and at higher pressure a combination of 13.64 km/s/fringe and 5.4603 km/s/fringe. Free-surface velocities for the shots reported here which used a diamond tamper are shown in Extended Data Figure 5. In all shots the sample is initially shocked to 0.1 TPa, which is the elastic limit of diamond, and then ramp compressed. By the time the compression wave reaches the free surface, the ramp has partially steepened into a shock, as predicted by the radiation-hydrodynamic simulations (Extended Data Figure 5c).

The diamond equation of state along a ramp-compression pathway is well-known from previous experiments[23,33], so the stress history across the bulk of the sample can be inferred from this velocity using the method of characteristics[31].

Stress Uncertainty: Uncertainty in the stress state of the sample at the time of the experiment comes from several sources: (1) Uncertainty in the diamond free surface velocity measurement coming from spatial variation across the sample and a velocity resolution of 3% of the velocity/fringe. These combined sources contributed between 0.015-0.040 TPa to the uncertainty from shot to shot. (2) Uncertainty in the diamond equation of state used to perform the characteristics analysis. The data shown in this report was analyzed using the ramp equation of state measured for full-density diamond up to 0.8 TPa[33], extrapolated to the 2 TPa range by assuming a linear relationship between the longitudinal sound speed and particle velocity. The error in the diamond ramp EOS was also extrapolated to 20 Mbar and propagated, contributing 3.5% to the stress uncertainty reported here. The choice of ramp equation of state is a systematic uncertainty which is not explicitly included in the error bar. If the 5 TPa ramp equation of state measured for nanocrystalline diamond[23] is used, the resulting stresses are systematically lower (by up to 0.04 TPa) near 1 TPa, and within 0.005-0.01 TPa near 2 TPa, because of the similarity in sound speed at those conditions. (3) Uncertainty in the strength of diamond, which introduces a systematic error in the characteristics analysis. The analysis method assumes that the pressure releases along the same pathway as the compression, ignoring any change in strength. A test with radiation hydrodynamic simulations suggests that this assumption could result in an underestimate of the stress on the order of 0.05 TPa (Extended Date Figure 5b). We have consequently added a 0.05 TPa contribution to higher-stress error bar. (4) Uncertainty in the timing of the x-ray source due to the timing accuracy of the streak camera diagnostic which registered it, and to the finite rise and decay times of the x-ray emission, which contributed between 0.002 and 0.01 TPa to the total uncertainty. There is also a contribution from the uncertainty in the target layer thicknesses due to accuracy of the metrology and to the variation in thickness across the part. This turned out to be negligible, since the metrology accuracy is <0.5 μm, and the diamond parts are parts are very flat (<0.5 μm-variation across the region probed in the experiment).

There is a spread of stress states in the sample over the duration of the x-ray pulse which varies from shot to shot, depending on how accurately the x-ray source was timed. Stresses reported here are the mean of a histogram of those stress states. Normally we consider that the width of this histogram is correlated with the (symmetric) width of the x-ray diffraction peaks and does not contribute to the stress uncertainty. In this case however, because there is some uncertainty in which region of the thick sample is contributing to the diffraction pattern, the histogram width may actually be correlated with an additional source of uncertainty. It is unclear how to accurately include this contribution in our error bar, so we summarize the full-width-half-maximum of the histogram of stress states across the sample, over the duration of the XRS pulse, in Extended Data Table 1.

X-ray Diffraction Measurement The TARDIS (TARget Diffraction In-Situ) x-ray diffraction diagnostic[29] is a half-cylinder-shaped chamber made of thick tantalum-tungsten alloy, lined with 3 image plates. The metal foil used for the x-ray source is mounted to an arm attached to the front of the diagnostic. The sample and collimating pinhole are mounted on the front of the chamber and an aperture to allow entrance of the VISAR laser used for the velocity measurement is positioned on the opposite wall (Extended Data

Figure 1). Filter materials are layered on the image plates inside the chamber, to absorb unwanted low- and high-energy x-rays. 5-15 μm-thick layers of Ge or Zr (material chosen to match the x-ray source, since their He- α energies fall below their absorption edges) are the primary filters, and in several shots an additional 75-150 μm Al is added, to further block the low-energy ablation plasma x-rays. 10- and 15-μm-thick Ge filters are made by depositing 5 μm of Ge onto 25 μm-thick layers of kapton, and stacking multiples to make up the full thickness. A 500 μm-thick rigid polycarbonate shell is made to fit into the TARDIS diagnostic box, supporting the filter layers and housing a thick tantalum canister around the direct x-ray beam, to attenuate it so that it does not overly saturate the image plate, and to block scattered x-rays and fluorescence that it generates.

After the shot the diagnostic is retrieved, disassembled and image plates scanned. The quasi-monochromatic x-ray scattering from the sample is time-resolved because of the duration of the x-ray pulse, but the image plate data is time-integrated so it registers all scattered x-rays from the ablation plasma (as well as Bremsstrahlung radiation from the x-ray source and subsequent fluorescence) which occur over the course of the experiment and may penetrate the filtering. For the high drive intensities necessary to achieve 2 TPa pressures, the ablation plasma background on the image plates is extreme (Extended Data Figure 4b), and good background subtraction metbods are therefore critical. We have used the SNIP method presented in detail by Rygg et al.[29] and it is shown applied to one of the high-pressure shots in Extended Data Figure 6. In addition to a smoothly-varying background from the broad-band radiation through the pinhole, there are many additional sources for spurious features in the image plates, which compete with the Bragg scattering. An example is shown in Extended Data Figure 7.

Structure Uncertainty The uncertainty in diffraction peak angles due to image plate calibration is 0.2°, as described in[?] . Uncertainty in the peak centroid location from peak fitting is negligible for the (111) peak (0.01°) but is near 0.1° for the (220) peak, which rises barely above the noise, in several cases. We consider an additional source of uncertainty based on the fact that there is a large thickness of diamond material (pusher, sample, tamper) in the target which may contribute to the x-ray diffraction signal. We do not rule out that some of this diamond material may be melted, either due to heating from the drive on the side closest to the laser, or due to shocks forming on the side closer to the diagnostic. Additionally, scattering from the diamond window has an outsize contribution to the average intensity in some cases because of the strong texture in the crystal. This large potential sample volume and uncertainty in which part contributes most significantly to the diffraction signal means that we consider a range of possible distances between the sample and the detector, which has an impact on the calibration. This introduces an angle-dependent uncertainty of 0.05° for the (111) peak and 0.2° for the (220) peak. There is an additional source of uncertainty for shot N180214 because this shot used a Zr x-ray source, and it reflects the fact that the precise x-ray source energy is not well known. The reported numbers assume an x-ray energy of 16.25 keV, which is the average of the two Zr heliumlike emission lines, as is done for the case of Ge. However, there is some evidence that the Zr is not being fully ionized to the He-like emission so the energy may be peaked lower; nearer to 16 keV[52]. We represent this uncertainty with an asymmetric error bar. A rigorous assessment of uncertainty in peak angles is necessary to rule out other candidate structures (Extended Data Figure 8). The same sources of uncertainty are reflected in the density error bars, which also include the error in the least squares fitting of the diffraction peaks to the FC8 structure.

DATA AVAILABILITY

The data that support the findings of this study are available from the corresponding author upon reasonable request.

AUTHOR CONTRIBUTIONS

J.S.W. and J.H.E. conceived the work, A.L., D.M., J.R.R., R.F.S., M.G.G., P.G.H., A.H. and M.J.S. performed the experiments, D.G.B. designed the laser pulse shapes, A.L. analyzed the data with assistance from J.R.R., J.H.E., D.E.F., D.E. and J.B. D.C.S., F.C., C.E.W., R.G.K., J.M.M., R.E.R. and G.W.C. contributed to the design of the work and interpretation of the data. A.L. and J.S.W. wrote the paper. All coauthors commented critically on the manuscript.

COMPETING INTERESTS

The authors declare that they have no competing financial interests.

CORRESPONDENCE

Correspondence and requests for materials should be addressed to A.L. (email: lazicki1@llnl.gov/jenei2@llnl.gov).